

Cosmological Evolution of Long Gamma-ray Bursts and Star Formation Rate

Vahé Petrosian^{1,2} Ellie Kitanidis³ and Daniel Kocevski⁴

¹*Department of Physics and KIPAC, Stanford University, Stanford, CA 94305, USA*

²*Department of Applied Physics, Stanford University, Stanford, CA 94305, USA*

³*Department of Physics, UC Berkeley, Berkeley, CA USA*

⁴*NASA Goddard Space Flight Center, College Park MD*

ABSTRACT

Gamma-ray bursts (GRBs) by virtue of their high luminosities can be detected up to very high redshifts and therefore can be excellent probes of the early universe. This task is hampered by the fact that most of their characteristics have a broad range so that we first need to obtain an accurate description of the distribution of these characteristics, and specially, their cosmological evolution. We use a sample of about 200 *Swift* long GRBs with known redshift to determine the luminosity and formation rate evolutions and the general shape of the luminosity function. In contrast to most other forward fitting methods of treating this problem we use the Efron Petrosian methods which allow a non-parametric determination of above quantities. We find a relatively strong luminosity evolution, a luminosity function that can be fitted to a broken power law, and an unusually high rate of formation rate at low redshifts, a rate more than one order of magnitude higher than the star formation rate (SFR). On the other hand, our results seem to agree with the almost constant SFR in redshifts 1 to 3 and the decline above this redshift.

Subject headings: Gamma rays: bursts-cosmology: early universe-stars: formation-general methods: statistical

1. Introduction

Observations of increasing numbers of gamma-ray bursts (GRBs) with measured redshifts, up to $z \sim 10$, by instruments on board *BeppoSAX*, *HETE*, *INTEGRAL*, and in particular *Swift*, have stimulated many uses of them as cosmological probes either as “standard Candles” (SC) for determination of global cosmological parameters, such as density parameters and equations of state, or as probes of the early phases of the universe such as reionization, or star formation rate (SFR) and cosmic metallicity evolution (CME) at high redshifts. Unfortunately, most intrinsic *distance dependent* characteristics of GRBs, such as their peak luminosity, total emitted energy, etc, have a broad distribution making them unsuitable as SC. However, there has been several attempts to discover some distance dependent characteristic that shows a well defined correlation with another *distance independent* characteristic, which can then be used to determine distances as in Cepheid variables or type Ia supernovae. Example of such relations for GRBs are the correlations between lag and luminosity (Norris et al. 2000), the variability and luminosity (Reichart et al. 2001), and the peak energy E_p of the νF_ν spectrum and the total (isotropic) gamma-ray energy \mathcal{E}_{iso} (Amati et al. 2002; Lamb et al. 2004; Attiea et al. 2004) or the beaming corrected energy \mathcal{E}_γ (Ghirlanda et al. 2004). For a more general review see Xiao & Schaffer (2009).

There are, however, many uncertainties in the claimed relations rendering the cosmological tests unreliable. First, it is now clear that these characteristics have broad distributions and that the correlations are

not simple one-to-one relations that is sometimes claimed and do not have the small dispersion required for precision cosmological tests. Instead, most of the correlations are statistical in nature, as originally predicted by Lloyd et al. (2000) long before any redshifts were measured, and not valid for the GRB population as a whole (Nakar & Piran 2004; Band & Preece 2005). Butler et al. (2009) stress that a careful accounting of observational selection effects is required, and suggest using the methods developed by Efron and Petrosian (EP for short, see below), to quantify the nature and degree of the correlations before any cosmological tests can be affected.

Secondly, even if there exists a one-to-one relation; e.g. $\mathcal{E}_{\text{iso}} = \mathcal{E}_0 \mathcal{C}(E_p/E_0)$, the relation between the cosmological parameters, such as matter and dark energy density parameters Ω_m and Ω_Λ and observed quantities, such as redshift z , flux $f(t)$ [or fluence $F = \int f(t)dt$] and E_p , are complicated. Here \mathcal{E}_{iso} is related to the total gamma-ray energy fluence F_{tot} as

$$\mathcal{E}_{\text{iso}} = 4\pi d_L^2 F_{\text{tot}}/Z, \quad \text{where} \quad d_L = (c/H_0)Z \int_0^z dz'/\sqrt{\Omega(z')} \quad (1)$$

is the luminosity distance, and $\Omega(z) = \epsilon(z)/\epsilon_0$ describes the evolution of the total energy density $\epsilon(z)$, of all substance.¹ In this case the cosmological parameters are related to the observations as

$$\left(\int_0^z \frac{dz'}{\sqrt{\Omega(z')}} \right)^2 = \left(\frac{H_0}{c} \right)^2 \left(\frac{1}{4\pi Z} \right) \left(\frac{\mathcal{E}_0 \mathcal{C}(E_p^{\text{obs}} Z/E_0)}{F_{\text{tot}}} \right), \quad (2)$$

which involves at least 2 unknown functions $\Omega(z)$ and $\mathcal{C}(E_p)$, and 3 more if the correlation function \mathcal{C} , and the scales \mathcal{E}_0 and E_0 evolve in time. Without a knowledge of the forms of the evolution functions $\mathcal{C}(E_p, z)$, $\mathcal{E}_0(z)$ and $E_0(z)$ precise determination of the $\Omega(z)$ is not possible. Most attempts to this end have assumed not only that the correlation function has small dispersion (e.g. $\mathcal{C}(E_p) \propto \delta(E_p - E_0)$) but also that it remains narrow at all redshifts (i.e. E_0 does not evolve), and that there is no luminosity or \mathcal{E}_{iso} evolution (i.e. \mathcal{E}_0 is a constant).

There has been some attempts to determine some aspects of the evolution (see e.g Li 2007), but most of these evolutionary trends have not been addressed. These evolutions, in principle, can be determined for an assumed cosmological model given a large enough sample. However, using such results to determine the cosmological model will be a circular and meaningless exercise. Thus, at this state of our knowledge, the use of the current GRB data for determining the global cosmological parameters seems premature. We need to learn more about the nature of the GRBs and the cosmological evolution of their characteristics before they can be used for this task. The immediate situation may be more akin to star forming galaxies and active galactic nuclei (AGNs), whose characteristics have also broad distributions and may evolve in time. This fact has shifted the focus of activity (both in galaxies, AGNs and GRBs) to the investigation of structure formation, the building process of the black holes, and to SFR and CME.

In recent years there has been increased activity in trying to use the existing GRB data to determine the shape and evolution of the luminosity function (LF), $\Psi(L, z)$, the GRB formation rate density (co-moving) $\dot{\rho}(z)$ (GRBFR for short), and its relation to the SFR or CME (see e.g. Porciani & Madau 2001; Natarajan et al. 2005; Daigne *et al.* 2006; Jakobson et al. 2006; Le & Dermer 2007; Salvaterra et al. 2009; Butler et al. 2010; Wanderman & Piran 2010; Howell et al. 2014). All these works use the forward fitting (FF) method, whereby the observed data, such as flux, fluence and redshift distributions are fit to prediction

¹Here $Z \equiv 1 + z$, $\epsilon_0 = 3H_0^2 c^2 / (8\pi G)$ and $\Omega(z) = \Omega_m Z^3 + \Omega_\Lambda$. In what follows we use a Hubble constant $H_0 = 70$ km/(s Mpc), and assume a flat universe with $\Omega_m = 0.3$ for matter and $\Omega_\Lambda = 0.7$ for the cosmological constant.

of models with some assumed *parametric forms* for the numerous functions [LF, $\dot{\rho}(z)$, spectrum] and their evolutions. For example, a common practice is to ignore luminosity evolution (see, however, Salvaterra et al. 2012) and assume a GRBFR similar to the SFR, a power-law LF with breaks, Band spectrum with unique values of the high and low energy indexes, etc. A more objective procedure would be to determine these characteristics from the data directly and, as much as possible, *non-parametrically*. The statistical methods developed by Efron and Petrosian are designed exactly for this kind of analysis and have been used for analysis of cosmological evolutions of quasars (Maloney & Petrosian, 1999; Singal et al. 2011; Singal et al. 2013), GRBs (Lloyd et al. 1999); Kocevski & Liang 2006; Dainotti et al. 2013) and blazars (Singal et al. 2012; Singal et al. 2014).²

In this paper we apply these method to data from *Swift* on long GRB with known redshifts with the aim of determining the cosmological evolution of the general LF which means the luminosity and formation rate variation with redshift. This parallels very closely with an earlier work using pre and early *Swift* data which formed a chapter of Aurelien Bouvier’s PhD thesis at Stanford (Bouvier 2010). The results of this work can also be found in Petrosian et al. (2013). In the next section we describe the data we use and in §3 we present a brief description of the method as applied to these data. The results are presented in §4 and a brief summary and discussion is given in §5.

2. Swift Data and Selection Effects

Over the last decade, the Burst Alert Telescope (BAT) on board the *Swift* satellite has detected more than 800 long GRBs with peak fluxes in the 15-150 keV energy band and above the threshold flux $f_{p,\text{lim}} \sim 2 \times 10^{-8}$ erg/(s cm²). Approximately, 90% by the *X-ray Telescope* (XRT) and about one third by both XRT and the *Ultraviolet/Optical Telescope* (UVOT). Redshifts obtained for over 250 *Swift* GRBs from these instruments and the follow up observations they enable on larger, ground-based telescopes. Fig. 1 shows scatter diagram of luminosities and redshifts for 253 long GRBs, taken from Nysewander et al. (2007), Butler et al. (2009), and NASA’s online burst archive, which collates data from Evans et al. (2009) and the Gamma-ray Coordination Network circulars.

From the redshifts and the observed peak gamma-ray energy flux f_p , integrated over the observed *Swift*-band (15–150 keV), we calculate the peak luminosity for the assumed cosmological model and K-corrected for the same rest frame energy band as³

$$L = 4\pi d_L^2(z, \Omega) f_p / K \quad \text{with} \quad K(Z) = \frac{\int_{15Z \text{ keV}}^{150Z \text{ keV}} E f(E) dE}{\int_{15 \text{ keV}}^{150 \text{ keV}} E f(E) dE}. \quad (3)$$

The spectra $f(E)$ are fitted to either a power law $f(E) = A(\frac{E}{100})^\alpha$, a power law with an exponential cutoff

²Codes for application of these methods can be found at <http://www.inside-r.org/node/99623> and cran.r-project.org/web/packages/DTDA/DTDA.pdf.

³Note that this definition of the K-correction follows the original definition that can be found in e.g. Peebles (1993). Sometimes the inverse of this is use relating a fixed rest frame energy band to a variable observed band, e.g Bloom et al. (2001) in which case $K(Z) = \frac{\int_{15 \text{ keV}/Z}^{150 \text{ keV}} E f(E) dE}{\int_{15 \text{ keV}}^{150 \text{ keV}} E f(E) dE}$. For a power law spectrum these give identical results but could be different when there are significant spectral deviation from a simple power law.

$f(E) = A(\frac{E}{100})^\alpha e^{-\frac{(2+\alpha)E}{E_p}}$, or the Band model

$$[f(E) = \begin{cases} A(\frac{E}{100})^\alpha e^{-\frac{(2+\alpha)E}{E_p}} & E < E_{br} \equiv \frac{(\alpha-\beta)E_p}{2+\alpha} \\ A(\frac{E}{100})^\beta e^{\beta-\alpha} (\frac{E_{br}}{100})^{\alpha-\beta} & E \geq E_{br} \end{cases} \quad (4)$$

In Figure 1 the dotted and solid (black) curves show the truncation $L > L_{\min}(z) = 4\pi d_L^2(z, \Omega) f_{\min}/\bar{K}$ due to two *fiducial peak flux thresholds* f_{\lim} and for \bar{K} correction calculated for an average spectrum. To insure a higher completion level in what follows we use the larger limiting flux of $f_{\lim} = 2 \times 10^{-8}$ erg/(s cm²) that includes 207 sources. The smoothed redshift distribution of this subsample is shown by the dotted (red) curve in the left panel of Fig. 4. The truncation induces a strong luminosity-redshift correlation, $L \propto Z^{3.3}$, shown by the dashed (green) line, which complicates the determination of the true intrinsic correlation, namely the luminosity evolution.

However, in addition to the bias involved in the detection of the prompt emission, the measurement of the redshift can introduce further truncations. X-ray and optical afterglows are vital for timely and accurate burst localization and redshift measurement. It is difficult to quantify the optical selection criterion. But as discussed in §4.3, we can include in our analysis the effects of X-ray selections. Since the optical and X-ray afterglow fluxes show relatively strong correlation, inclusion of X-ray selection effects may to some degree alleviate the problem of the optical selection effects.

3. Methods and Approach

The problem under consideration here requires determination of multi variate distribution from data truncated by observational selection effects. We will demonstrate our approach for determination of single LF and its evolution; $\Psi(L, z)$ from a flux limited sample such as that shown in Fig. 1. Without loss of generality, we can write the LF as

$$\Psi(L, z) = \dot{\rho}(z)\psi[L/g(z), \alpha_i]/g(z), \quad (5)$$

where, in addition to the GRBFR $\dot{\rho}(z)$, we have introduced $g(z)$ and α_i to describe luminosity and shape evolutions, respectively. Given sufficiently large sample one can determine all three evolutions. Our experience with evolution of the LF in other extragalactic sources such as quasars and blazars indicates that the least variable among these is the shape parameter(s). Thus, because of the limitations of the current GRB data we will focus here only on the GRBFR and luminosity evolutions and assume constant shape parameters. The truncation or bias introduced by the flux limit [$f > f_{\lim}$ or $L > L_{\min}(z) = 4\pi d_L^2(z) f_{\lim}/K(z)$] is known as the **Malmquist Bias**. Many papers have been written to correct for this bias in astronomical literature (Malmquist 1925); Eddington 1940; Trumpler & Weaver 1953; Neymann & Scott 1959). Most of these early procedures assumed simple parametric forms (e.g Gaussian) distributions. However, since the discovery of quasars the tendency has been to use non-parametric methods: e.g $\langle V/V_{\max} \rangle$ (Schmidt 1972; Petrosian 1973) or the C^- (Lynden-Bell 1971). For a more detailed description see review by Petrosian (1992). All these methods however, suffer from a major shortcoming because they assume that the variables are independent or uncorrelated, or that the LF is separable; $\Psi(L, z) = \psi(L)\dot{\rho}(z)$. This ignores luminosity evolution and is an assumption that is made commonly for GRBs which turns out to be incorrect (see below).

Thus, the first task should be the determination of the correlation between the variables. Unfortunately, most past works dealing with determination of the GRB LF or GRBFR (those mentioned above and others;

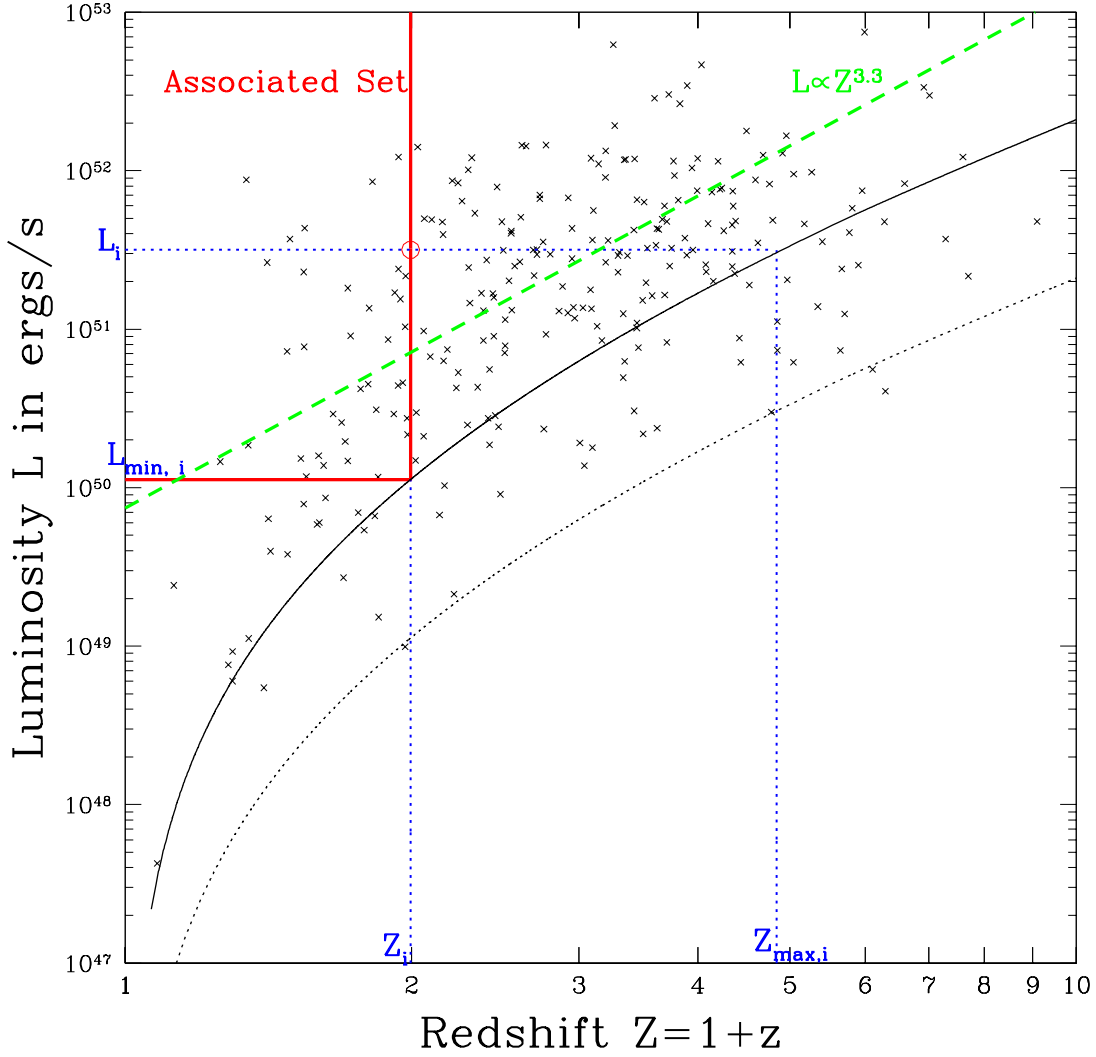


Fig. 1.— K-corrected Luminosity vs. redshift. The solid and dotted (black) curve shows the truncation due to a flux limits of $f_{\text{lim}} = 2 \times 10^{-8}$ and 2×10^{-9} erg/(s cm²), respectively. In our analysis we use the larger and more conservative limit. The dashed (green) line shows the best fit luminosity evolution to the raw data (data points above the solid curve. Most of this correlation is due to the truncation. The solid (red) vertical and horizontal lines define the boundaries of the associated set (in this case M_i) of the source marked by the red circle. The dotted (blue) lines and letters show the luminosity and redshift of the source and the maximum redshift and the minimum luminosity, defined in Eq. (6), that this source can have and still be in the sample.

e.g. Kistler et al. 2007; Li 2008) omit this crucial step, which, as described below can lead to an incorrect GRBFR. A commonly used non-parametric method for determining correlations is the Spearman Rank test.

This method, however, fails for truncated data. Efron & Petrosian (1992) developed a novel method to account for this truncation. The gist of the method is to determine the rank R_i of each data point L_i (or z_i) among the N_i (or M_i) members of its *associated set*, or its largest un-truncated subset. The region bounded by the red lines in Fig. 1 depicts the boundary of this set for the data set L_i, z_i identified by the red circle. This is for ranking in redshifts (from low to high values) and the set includes M_i sources with $z_j < z_i$ and $z_{\max,j} > z_i$ (or $L_j > L_{\min,i}$). In an analogous manner one can define the set of N_i sources with $L_j > L_i$ and $L_{\min,j}(z) < L_i$ (or $z_j < z_{\max,i}$ for ranking the luminosities from above. These limiting values, also shown in Fig. 1, are given as

$$L_{\min,j} = 4\pi d_L^2(z_j) f_{\text{lim}} / \bar{K}(z_j) \quad \text{and} \quad L_j(z) = 4\pi d_L^2(z_{\max,j}) f_{\text{lim}} / \bar{K}(z_{\max,j}). \quad (6)$$

Then using a test statistic, e.g. Kendell’s tau defined as $\tau = \Sigma_i(R_j - E_j) / \sqrt{\Sigma_i V_j}$, one can determine the degree of correlation. Here E_j and V_j are the expectation and variance of the ranks. A small value ($\tau \ll 1$) would imply independence, and $\tau > 1$ would imply significant correlation. In the latter case one can redefine the variables, e.g. define a “local” luminosity $L' = L/g(z)$ [with $g(0) = 1$] using a parametric form, e.g. $g(z) = (1 + z)^k$, and calculate τ as a function of the parameter k .⁴ The values of k for which $\tau = 0$ and $\tau = \pm 1$ give the best value and one sigma range for independence.

Once independence is established then one can use the above mentioned non-parametric methods ($\langle V/V_{\max} \rangle$ or the C^-) to determine the mono-variate distributions; local LF $\psi(L')$ and the formation rate evolution $\dot{\rho}(z)$. We will use the C^- method which builds up the cumulative distributions of both variables L and z defined as

$$\dot{\sigma}(z) = \int_0^z \frac{\dot{\rho}(z')}{Z'} \frac{dV(z')}{dz'} dz' \quad \text{and} \quad \phi(L') = \int_{L'}^{\infty} \psi(x) dx \quad (7)$$

point by point non-parametrically, again using the concept of the *associated set*. For example $\phi(L_i) = \prod_{j=2}^i (1 + 1/N_j)$. The cumulative functions can then be differentiated to get ψ and $\dot{\rho}$ using the derivative of the $V(z)$, the co-moving volume up to z .

The observed redshift distribution is related to the cumulative functions as

$$\frac{dN}{dz} = \frac{d\dot{\sigma}(z)}{dz} \phi[L'_{\min}(z)] \quad \text{with} \quad L'_{\min}(z) = \frac{4\pi d_L^2(z) f_{\min}}{\bar{K}(z)g(z)}, \quad (8)$$

where $\phi[L'_{\min}(z)]$ represents the effects of the truncation and $d\dot{\sigma}(z)/dz$ gives the true redshift distribution of the parent population; i.e. what one would observe in the absence of truncation (i.e. when flux thresholds $f_{\text{lim}} \rightarrow 0$).

It should also be noted that, this method is not limited to a simple flux limited data but, as shown in Efron & Petrosian (1999), it can deal with truncations from both below and above, or with the most general truncation situation where each data point, say $[L_i, z_i]$, has its individual upper and lower limits, $[L_{i,\min} < L_i < L_{i,\max}$ and $z_{i,\min} < z_i < z_{i,\max}]$. We will not be dealing with such complications here, since our data is truncated from below only.⁵

In appendix A we apply this method to a flux limited sample selected from a parent simulated sample with known characteristics of the LF and evolution, and demonstrate that we recover the input characteristics accurately.

⁴Note that for each k the limiting values $L_{\min,j}(z_{\max,j})$ and associated sets $N_j(M_j)$ are calculated anew.

⁵We note, however, that this is an enormous advantage because it allows one to combine data from many different regions of sky with different backgrounds and even from different instruments obtained with different selection criteria.

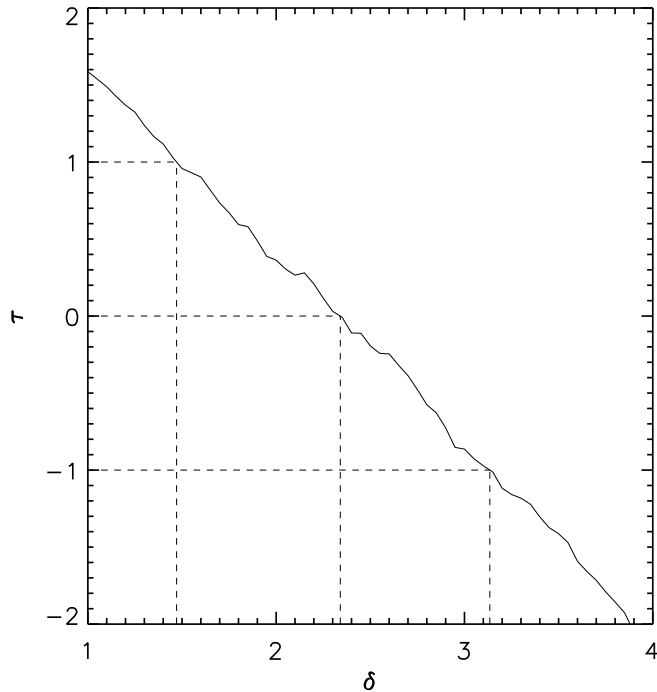


Fig. 2.— Variation of Kendall’s τ statistics with the evolution index δ showing independence for $\delta = 2.33$ with one sigma range 1.48 to 3.12. We set $\delta' = \delta$ and $Z_{\text{cr}} = 3.5$ in Eq. (9).

4. Results

4.1. Luminosity Evolution

As stressed above, the first task is to carry out test of the independence of L and z and determine the luminosity evolution. As shown above the raw data shows strong correlation $L \propto Z^{3.9}$. Using the associated sets to account for the truncations we find a Kendall’s $\tau \sim 3.5$ indicating the presence of a strong intrinsic correlation (i.e. luminosity evolution). The form of the evolution can be determined parametrically. The form often used is $g(z) = Z^\delta$ which is appropriate for low and intermediate redshifts. But at higher redshifts this becomes excessively large considering the fact that the time intervals $dt = dZ / (Z\sqrt{\Omega_M Z^3 + 1 - \Omega_M})$ decreases rapidly with increasing redshifts for $Z > 3$. Based on our experience in treating the evolution of the quasars we use the following, that has a slower luminosity evolution for $Z > Z_{\text{cr}}$

$$g(z) = \frac{Z^\delta \times Z_{\text{cr}}^{\delta'}}{Z^{\delta'} + Z_{\text{cr}}^{\delta'}}. \quad (9)$$

After some trial and error we settled on $Z_{\text{cr}} = 3.5$ and $\delta' = \delta$, leaving us with one free parameter. We then define the “local” luminosity $L' = L/g(z)$ (and the truncation curve $L'_{\text{min}}(z) = L_{\text{min}}(z)/g(z)$) and calculate the statistic τ as a function of δ . Fig. 2 shows the results indicating independence of L' and z for $\delta = 2.3$ with the one sigma range [1.5 – 3.1]. This is significantly less than the raw index ~ 4 , but still considerable evolution; factors of 4.0, 7.8 and ~ 11 at redshifts 1, 2 and 3, respectively. This is in agreement with recent

results using FF methods (e.g. Salvaterra et al. 2012) and earlier results using the Efron-Petrosian method on pseudo-redshift samples (Lloyd-Ronning et al. 2002; Yonetoku et al. 2004; Kocevski & Liang 2006) and samples with redshift (Petrosian et al. 2013).

4.2. The Luminosity Function

Transferring the observed $L - z$ scatter diagram to the local luminosity $L' - z$ diagram we can now determine the local LF $\psi(L')$ using the C^- method. Since we have assumed that the shape of the LF is invariant this function when shifted in luminosity by $g(z)$ describes the LF at all redshifts. The left panel of Fig. 3 shows the cumulative local LF $\phi(L')$ build up point by point starting with the highest observed luminosity (filled points). For comparison we also show the raw cumulative distribution (open circles) showing the correction due to truncation obtained by our method. As shown in Appendix B one can also obtain a histogram of the differential LF

$$\psi(L') = -\frac{d\phi(L')}{dL'} = -\frac{\phi(L')}{L'} \frac{d\log \phi(L')}{d\log L'} \quad (10)$$

directly from the data. However, because of the paucity of the data and the random nature of the luminosities, their separation (e.g. $\delta \log L_i = \log(L_{i-1}/L_i)$) has a large dispersion yielding a noisy differential LF. Instead we obtain the differential LF by taking the derivative of appropriately smoothed curve fitted to $\phi(L')$. As shown by the dashed (red) and dotted (green) curves in Fig. 3 (left) a smooth broken power law or a power law with exponential cutoff provide adequate fit to the cumulative LF. Derivatives of this give a similar description for the differential LF. For example the indices -0.5 and -2.2 of $\phi(L')$ means that the differential luminosity function can also be fitted to a broken law with indices $d\log \psi/d\log L' \sim -1.5$ and -3.2 . This is a steeper LF, especially at the high end, than some recent results based on FF method; e.g. Howell et al. (2014) obtain indexes $[-0.95, -2.59]$, and Salvaterra et al. (2012) obtain indexes $[-1.5, -2.3]$.

4.3. Formation Rate Evolution

From the $L' - z$ scatter diagram we can also obtain the GRBFR evolution. The cumulative rate evolution $\dot{\sigma}(z)$ is shown by the filled points on the right panel of Fig. 3. This is obtained point by point starting with the lowest redshift. Again, for comparison we also show (open points) the raw observed cumulative distribution $N(< z) = \int_0^z (dN/dz) dz$. On the left panel of Fig. 4 we compare the smoothed differential observed redshift distribution dN/dz (dotted red) with the true distribution $d\dot{\sigma}(z)/dz$ (solid, black), obtained from the derivative of a smooth solid (black) curve fitted to $\dot{\sigma}(z)$ on Fig. 3 (right). Both of the above comparisons show that observations miss many intermediate and high redshift sources due to truncations affected by the gamma-ray threshold. These curves are normalized at low redshifts where the effect of truncation is expected to be minimal. A proper normalization can be carried out using total population counts like the so-called $\log N$ - $\log S$ diagram, which is beyond the scope of this paper.

The co-moving GRBFR evolution is obtained as

$$\dot{\rho}(z) = Z \frac{d\dot{\sigma}(z)/dz}{dV(z)/dz}. \quad (11)$$

This is shown by the solid (black) curve on the right panel of Fig. 4. In this figure we also show the raw GRBFR that one would obtain ignoring the truncation (dotted, red), i.e. using the observed dN/dz instead

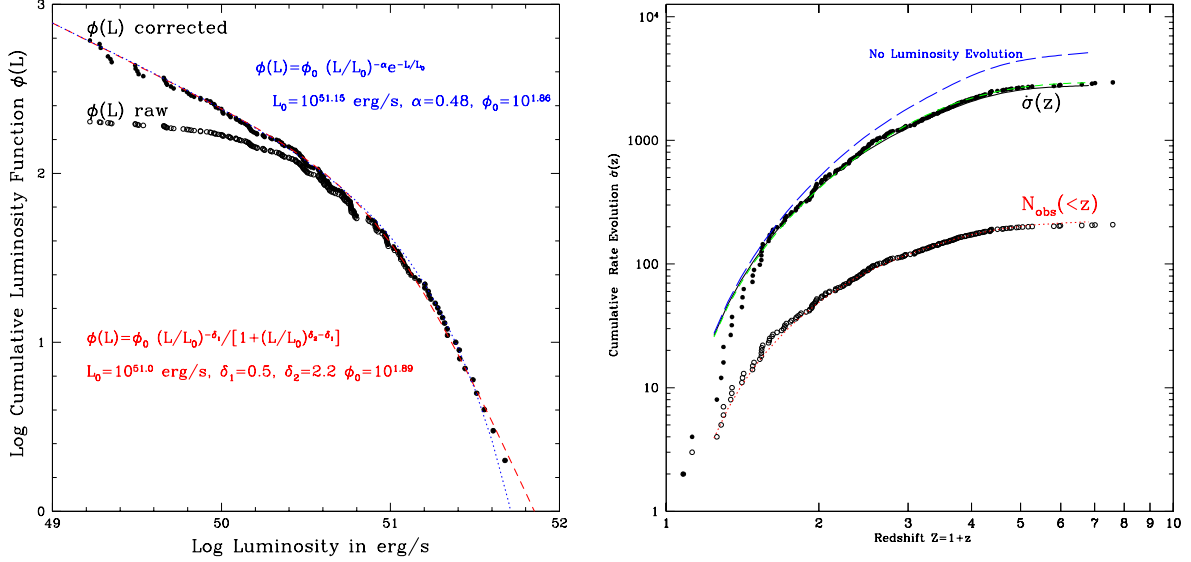


Fig. 3.— **Left:** The cumulative LF. The filled points shows the cumulative local LF $\phi(L')$ while the open points shows the cumulative distribution obtained ignoring the effects of the truncation. We have omitted 5 GRBs with $L < 10^{49}$ erg/s. The dashed (red) curve shows a broken power law fit with indices -0.5 and -2.2 above and below $L_0 = 10^{51}$ erg/s and the dotted (blue) curve shows a fit to Schechter function; a power-law with exponential cutoff. **Right:** The cumulative rate evolution $\dot{\sigma}(z)$ versus redshifts corrected for selection effects due to the γ -ray flux limit: filled points with solid (black) line a smoothed fit. The very similar dashed (green) curve is obtained using both *gamma* and X-ray threshold effects. The long-dashed (blue) is obtained ignoring luminosity evolution. The open points, and fitted dotted (red) curve, shows the observed cumulative distribution $N(<z)$, which of course does not include effects of the truncation.

of $d\dot{\sigma}(z)/dz$ in Eq. (11). As expected this gives much lower rate at higher redshifts. We have also calculated GRBFR evolution ignoring the luminosity evolution, i.e. determining the distributions from the $L - z$ data shown in Fig. 1 instead of $L' - z$ scatter diagram. This is shown by the dashed (blue) curves in Figs. 3 and 4. As evident ignoring the luminosity evolution overestimates the required GRBFR. This is the reason that some of earlier works (cited above) that ignored luminosity evolution obtained a high GRBFR at high redshifts, higher than the observed SFR. Again we have normalized these rates at low redshifts ($z < 1$) where the observational selection effects are smallest.

All of the above results are obtained including only the effects truncation due to prompt γ -ray detection threshold. As mentioned in §2, other observational selection effects, arising in the process of localization and securing redshifts, add more truncations. In particular the threshold of X-ray detection, the first crucial step for determination of the redshift, is an important factor. Based on the X-ray flux data from Racusin et al. (2011; private communications), we use a conservative limit of $\sim 2 \times 10^{-13}$ erg/(s cm²) (in the 0.2-10 keV range and at 11 hrs after the trigger) to determine how this additional selection bias affects our result. To this end we have repeated the above calculations using the effects of both gamma-ray and X-ray thresholds. This extra truncation redefines the *associated sets* which, as described above, for a single threshold consists of the set with $z_j < z_i$ and $z_{\text{max},j} < z_i$, where $z_{\text{max},j}$, defined in Eq. (6), is the maximum redshift the source

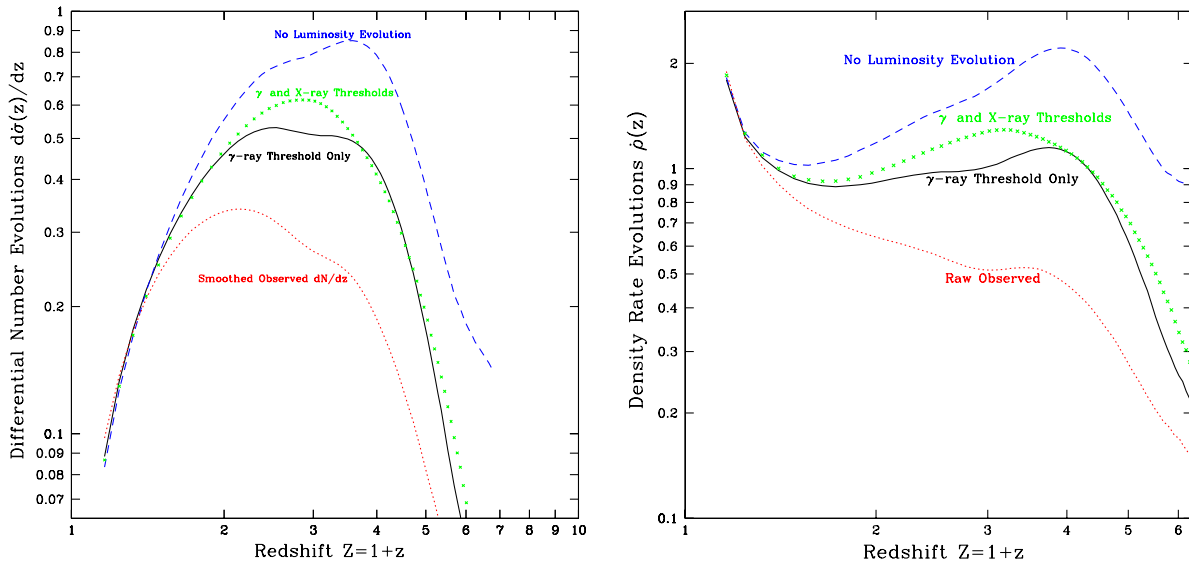


Fig. 4.— **Left:** Comparison of the observed redshift distribution dN/dz (dotted, red) with the intrinsic redshift distributions $d\dot{\sigma}/dz$ (solid, black) obtained from the differentiation of curves fitted to the cumulative distribution shown on the right panel of Fig. 3. The dashed (blue) curve shows the derived redshift distribution ignoring the luminosity evolution demonstrating the importance of inclusion of the luminosity evolution. The x points (green) are obtained including the effects of both gamma-ray and X-ray selection biases, as well of the luminosity evolution, as described in the text. This is very close to the black curve indicating that most of the selection bias is already accounted for by the correction for the gamma-ray threshold. These curves are normalized to redshifts $z < 1$ where the observational selection bias is expected to be small. **Right:** The density rate evolution obtained from the distributions on the left and Eq. (11) using the same color codes. The dashed (red) curve is obtained using the smoothed observed dN/dz which shows a much more rapid decline than the true rate obtained for γ -ray threshold only (solid black), both γ and X-ray thresholds (long-dash green). The dashed (blue) curve is obtained ignoring the luminosity evolution. All rates are normalized at $z < 1$.

with L_j, z_j can be moved to and still be in the sample. With two thresholds we now have two limiting redshifts. We use the minimum of the two to define the associated sets. The x points (green) on both panels of Figs. 4 show this results. These are very similar to the black curves obtained with the γ -ray threshold effects alone. This is encouraging because it may imply that the other selection effects in securing a redshift, which cannot be easily quantified, have also small effects. Comparing these with the raw (uncorrected) redshift distributions (dotted red curve) we conclude that most of the correction has already been accounted for by the gamma-ray threshold. We also note that, there is a strong correlation between X-ray and optical fluxes of *Swift* GRBs which indicates that the X-ray threshold may be good proxy for the optical selection effects.

Finally we note that a more rigorous approach to the multivariate nature of this problem would require us to obtain the evolution of the bivariate LF $\Psi(L_\gamma, L_X, z)$. As demonstrated in Singal et al. (2011) and (2013), the methods used in this paper for a single luminosity can be generalized to higher dimensions

without much difficulty. Similarly, if and when we understand the optical selection criterion, we can include optical luminosities as well in this multivariate distribution.

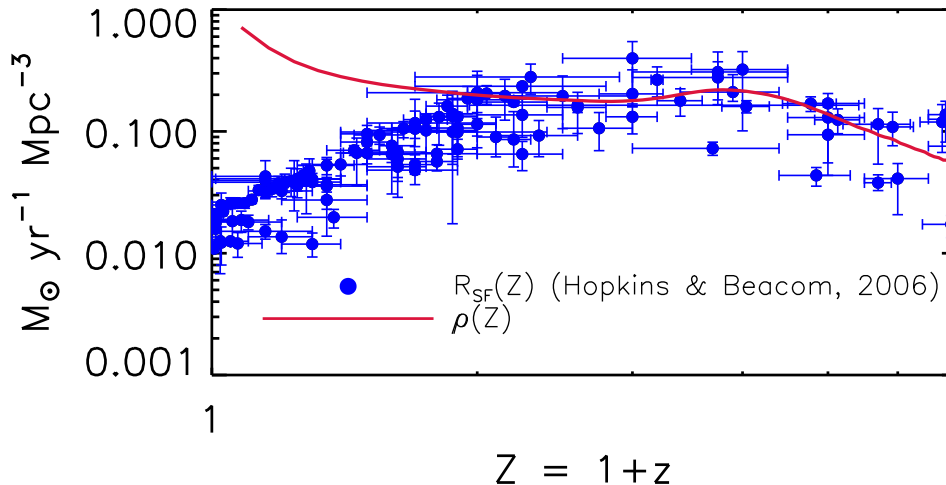


Fig. 5.— Comparison of the the derived GRBFR (dash-dotted, green curve on Fig. 4, right) and the SFR from Hopkins & Beacom (2006) normalized around redshift $z \sim 3$. The GRB rate (red) agrees remarkably well in the somewhat flat portion of the SFR rate and decays in a similar way at high redshifts. But at low redshifts it has a dramatically different shape and much higher rate.

5. Summary and Discussion

We have analyzed a sample of about 200 *Swift* flux limited long GRBs with known redshift using the non-parametric methods of Efron & Petrosian to obtain the general evolution of the luminosity function. Our results can be summarized as follows:

- We find that the observed strong correlation between the luminosity and redshift is not totally due to the effects of the flux limit but that there is significant intrinsic correlation indicating that GRBs have undergone a strong luminosity evolution at least up to $z \leq 3$ which can be approximated as $L \propto (1+z)^{2.3}$.
- Correcting for this evolution we then obtain the local LF which can be represented by a broken power law or a Schechter type function.
- We also find the true redshift distribution and the (co-moving) density rate evolution which starts at a maximum level at lowest redshifts, declines slowly up to $z \sim 1$ and merges into a plateau or an almost constant rate between redshift 1 and 3, and then shows a relatively steep decline at higher redshifts.
- Thus, we find that GRBs undergo both luminosity and density evolution; they were more luminous but less numerous in the past than today. Often the luminosity evolution is ignored which as shown here

gives an incorrect (higher) density rate evolution at high redshifts. This is the source of many claims that GRBFR is higher than SFR at higher redshifts (see, e.g. Kistler et al. 2008; Salvaterra et al. 2012; Wei et al. 2014). Robertson & Ellis (2012), and Dainotti et al. (2015) using afterglow emission, find a slower GRBR evolution, but their result also disagrees with ours because of their neglect of luminosity evolution.

- Most analyses of GRB evolution assume a formation rate similar to the SFR especially at low redshift, but with an increase rate at higher z 's. The additional evolution is derived by FF to the observed distribution of redshifts and fluxes. With our non-parametric method we obtain directly the GRB formation rate which is quite different than those derived by FF methods. As shown in the right panel of Fig. 5, our derived rate agrees very well with the SFR at redshifts $z > 1$, in particular in the plateau range $1 < z < 3$, and shows a similar rapid decline at higher redshifts. But at low redshifts $z < 1$ the GRB rate deviates by more than a decade from the SFR. This is puzzling because, according to the prevailing view that GRB formation is favored in low metallicity regions, one would expect a lower GRB rate in metal rich lower redshift galaxies.

There are many potential factors that can account for this discrepancy. The above results are based on the LF of the prompt emission and includes rigorously only the γ -ray threshold effects. But the data used involved also X-ray, UV and optical (space and ground based) measurement for localization and securing redshifts. We have included the X-ray detection threshold as best as can be done and find a small effect. The discrepancy at low redshifts remains large. It appears that the γ -ray threshold effects account for most of the data truncations. This is encouraging because it may indicate that less quantifiable UV and optical selection biases may have similarly small effects. It should be noted that these added selection effects are expected to be more important at high redshifts so that they, most likely, are not the source of the discrepancy at low redshifts. The fact that all curves in Fig. 4 have same shape at low redshifts supports this view.

Another possible factor may be the paucity of low redshift and low luminosity GRBs which dominate the shape of the nearby GRB rate. There have been some claims that low luminosity GRBs may belong to a separate class. However, as can be seen from Fig. 1, eliminating GRBs with $L_{\min} \leq 10^{49}$ erg/s from the list will affect only the result at $z < 0.4$ leaving a large discrepancy for $0.4 < z < 1$. This discrepancy, therefore, may have an important implication on the formation of long GRBs.

Acknowledgements: This work is partially supported by *Swift* guest investigator grants (NASA NNX12AE74G) and is based on Ellie Kitanidis's senior honor thesis at Stanford University (see <http://pur1.stanford.edu/xp981bq5003>).

Appendix A: Testing the Methods

To demonstrate the accuracy of our methods we have simulated a sample of sources with redshift and luminosity distributions similar to those of GRBs with specified form for the LF and density rate evolution but with no luminosity evolution. We have selected a flux limited subsample and applied the Efron-Petrosian methods to recover the intrinsic distributions. We recover no evolution (obtain Kendell's $\tau = 0$ for $k \sim 0.1$), and as shown in Fig. 6, the calculated cumulative distributions $\phi(L)$ and $\sigma(z)$, agree very well with the intrinsic distribution of the parent sample.

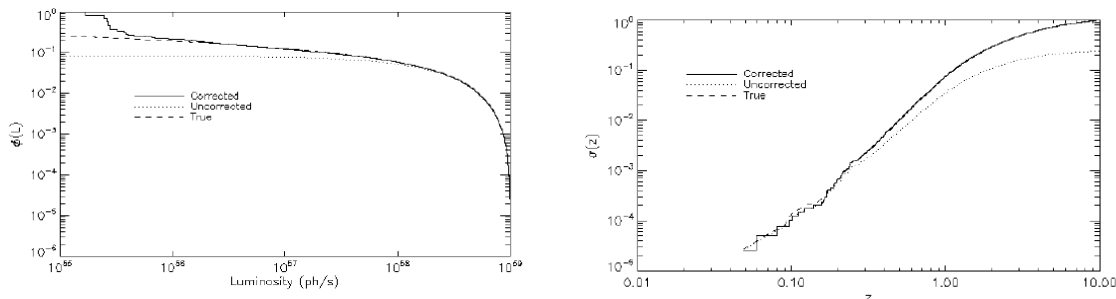


Fig. 6.— Comparison of the true intrinsic cumulative distributions (dashed) of a simulated sample (chosen to have characteristics similar to those of GRBs) with that of the flux limited “observed” sample (dotted) and that histogram obtained by our method that corrects for this selection bias. As evident the method reproduces the input forms extremely well, except at the extremities. **Left:** LF $\phi(L)$. **Right:** density rate $\dot{\sigma}(z)$.

Appendix B: Non-parametric Differential Distribution

As mentioned in §3 the Efron-Petrosian method gives a non-parametric and point by point description of the cumulative distributions. Our usual procedure is to fit such histograms to a smooth function and take its derivative to obtain the differential distributions. This is because one cannot differentiate a discontinuous histogram. Here we describe a point by point estimation of the differential distributions (using luminosity as an example) which can give us the histogram of the differential distribution.

The cumulative distribution up to and including each data point, say $\phi(L_i)$ is given as

$$\phi(L_i) = \prod_{j=2}^i (1 + 1/N_j) \quad (12)$$

where N_i is the number of data points in the associated set of point i (see Fig. 1). We can use two different estimator of the differential distribution $\psi(L) = -d\phi(L)/dL$.

We can use the estimator $\psi(L_i) = (\Phi(L_i) - \phi(L_{i-1})) / (L_i - L_{i-1})$ in which case it is easy to show that for $\delta_i \equiv L_{i-1}/L_i - 1$

$$L_i \psi(L_i) = \frac{\phi(L_i)}{\delta_i N_i} \times \frac{1}{(1 + 1/N_i)} \simeq \frac{\phi(L_i)}{\delta_i N_i} (1 - 1/N_i + \dots), \quad (13)$$

where the last equality is for $N_i \gg 1$.

Another estimator is obtain using the fact that Eq. (3) yields $\delta \ln \Phi(L_i) = \ln \phi(L_i) - \ln \phi(L_{i-1}) = \ln(1 + 1/N_i)$, which then gives

$$L_i \psi(L_i) = \phi(L_i) \frac{d \ln \phi(L_i)}{d \ln L_i} = \phi(L_i) \frac{\ln(1 + 1/N_i)}{\ln(1 + \delta_i)} \simeq \frac{\phi(L_i)}{\delta_i N_i} (1 - 1/(2N_i) - \delta_i + \dots), \quad (14)$$

which for $N_i \gg 1$ and $\delta_i \ll 1$ is equal to the first estimator.

We can similarly obtain the differential distribution $d\dot{\sigma}/dz$ and $\dot{\rho}(z)$.

Unfortunately, for a sparse data set with sometimes large gaps, such as that available for GRBs, not all N_i are large (especially at the two ends of the data, and the relevant quantities $\ln L - i$ or δ_i have large

dispersions. These fact introduce a large random noise so that we rely on smoothing and differentiation of the cumulative distributions. The above relation can be used for samples with dense and uniform coverage of the phase space.

REFERENCES

- Amati, L. et al. 2002, *A&A*, 390, 81
- Atteia J.-L. et al. 2004, AIP Conf. Proc. 727, p 37
- Band, D. L. & Preece, R. D. 2005 ApJ, 627, 319
- Bloom, J. S., Frail, D. A. & Sari, R. 2001, *AJ*, 121, 2879
- Bouvier, A. 2010, PhD Thesis, Stanford University
- Butler, N. R.; Kocevski, D. & Bloom, J. S. 2009, ApJ, 694, 76
- Butler, N. R.; Bloom, J. S.; Poznanski, D. 2010, ApJ, 711, 495
- Dainotti, M. G., Petrosian, V. et al. 2013, ApJ, 774..157
- Dainotti, M.G., Del Vecchio, R., Nagataki, S. & Capozziello, S., ApJ, 2015, 800, 31
- Daigne, F. et al. 2006, *MNRAS*, 372, 1034
- Eddington *MNRAS*, 1915, 73, 359 and 1940, 100, 354
- Efron, B. & Petrosian, V. 1992, ApJ, 399, 345 (**EP**)
- Efron, B. & Petrosian, V. 1999, J. Am. St. Assoc., 94, 824
- Ghirlanda, G. et al. 2004, ApJ, 613, L13
- Howell, E. J., Coward, D. M., Stratta, G., Gendre, B. & Zhou 2014 *MNRAS*, 444, 15
- Hopkins, a. M. & Beacom, J. F. 2006, ApJ, 651, 142
- Jakobsson , P. et al. 2006, *A&A*, 447, 897
- Kistler, M. D.,Yuksel, H.,Beacom, J. F. & Stanek,K. Z. 2008, ApJ, 673, L119
- Kocevski, D. & Liang, E. 2006, ApJ, 642, 371
- Lamb, D.Q. *et al.* . 2004, *New Ast. Review*, 48, 459
- Le, T. & Dermer, C. D. 2007, ApJ661, 394
- Li, L.-X. 2007, *MNRAS Letters*, 379, 55L
- Li, L.-X. 2008, *MNRAS*, 388, 1487
- Lloyd, N. M.& Petrosian, V. 1999, ApJ, 511, 550
- Lloyd, N. M., Petrosian, V. & Mallozzi, R.S. 2000, ApJ, 534, 227
- Lloyd, N. M., Fryer, C. L. & Ramirez-Ruiz, E. 2002, ApJ, 574,554
- Lynden-Bell, D. 1971, *MNRAS*, 155, 95
- Malmquist, K. G. 1920, *Medd. Lund. Obs.*, Ser. 2, No. 22
- Maloney, A. & Petrosian, V. 1999, ApJ, 518, 32
- Nakar, E. & Piran, T. 2004, *MNRAS*, 360, 73
- Natarajan, P. et al. 2005, *MNRAS*, 364, L8

- Neyman, J. & Scott, E. L. 1959, *Handbuch Der Physik*, Ed. S. Flugge, Springer-Verlag, Berlin, 53, 416
- Norris, J. P., Marani, G.F. & Bonnell, J.T. 2000, *ApJ*, 534, 248
- Nysewander, M. et al. 2009, *ApJ*, 701, 824
- Peebles, P. J. E. *Principles of Physical Cosmology*, 1993, Princeton Series in Physics, p330
- Petrosian, V. 1992, *Stat. Challenges in Modern Astro.*, p173 Eds. Feigelson & Babu, (N.Y. Springer-Verlag)
- Petrosian, V. 1973, *ApJ*183, 359
- Petrosian, V. et al. 2009; arXiv-0909.5051
- Porciani, C. & Madau, P. 2001, *ApJ*, 548, 522
- Reichart, D. E. et al. 2001, 552, 57
- Robertson, B. E. & Ellis, R.S. 2012, *ApJ*, 744, 95
- Salvaterra, R. et al. 2009, *MNRAS*, 397, 602
- Salvaterra, R. et al. 2012, *ApJ*, 794, 68
- Schmidt, M. 1968, *ApJ*, 151, 393
- Singal, J., Petrosian, V. & et al. 2011, *ApJ*, 743, 104
- Singal, J., Petrosian, V. & Ajello, M. 2012, *ApJ*, 753, 45
- Singal, J., Petrosian, V. & et al. 2013, *ApJ*, 764, 43
- Trumpler, R. J. & Weaver, H.F. 1953, *Statistical Astronomy*, Dover, N.Y.
- Wanderman, D. & Piran, T. 2010, *MNRAS*, 406, 1944
- Wei et al. 2014, *MNRAS* 3329, 439,
- Xiao, L. & Schaefer, B. E. 2009, *ApJ*, 707, 387
- Yonetoku, D., Murakami, T., Nakamura, T. R., Yamazaki, A. K. Inoue, & K. Ioka 2004 *ApJ*, 609, 953